DESIGN AND RETROFIT OF A LOW SOLIDITY DIFFUSER FOR A PIPELINE CENTRIFUGAL GAS COMPRESSOR APPLICATION

by

Michael B. Flathers

Manager, Gear Systems

Solar Turbines Incorporated

San Diego, California

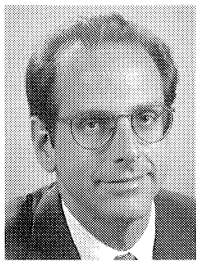

Michael B. (Mike) Flathers is Manager of Gear Systems at Solar Turbines, Incorporated, in San Diego, California. He is responsible for the design, development, configuration control, and support of gear products used on gas turbine engines and packages, including the specification of vendor gearboxes and low speed couplings. Previously, Mr. Flathers led the Aerodynamics and Performance Group in gas compressor engineering.

Prior to joining Solar in 1991, he held positions with Sundstrand Power Systems, where he was responsible for high pressure inert gas reciprocating compressors, and with Textron Lycoming, where he was responsible for higher pressure ratio centrifugal compressors.

Mr. Flathers received his B.S. degree (Mechanical Engineering) from Western New England College, his M.S. degree (Mechanical Engineering) from Rensselear Polytechnic Institute and is a member of Tau Beta Pi. He has authored or coauthored numerous technical publications, is a member of ASME, and is also a member of the Turbomachinery Committee of the International Gas Turbine Institute.

ABSTRACT

A high efficiency, single-stage pipeline centrifugal gas compressor, originally designed with a wedge-type vaned diffuser, was retrofitted with a vaneless diffuser along with two low solidity diffuser configurations in order to improve the operating flow range. The low solidity diffuser configurations included a flat-plate design and an airfoil-type design. The vaneless and flat-plate low solidity diffusers were derived from the existing wedge-type vaned diffuser, while the airfoil-type low solidity diffuser was designed specifically to match the existing impeller, but within the design envelope available for retrofit purposes. Computational fluid dynamics (CFD) was used to establish impeller discharge conditions, analyze candidate diffusers, and provide some guidance as to the expected operating range improvement. Both factory and field testing were conducted to verify the performance of the diffuser configurations. Test results indicated that the airfoil-type low solidity diffuser had the best overall efficiency and operating flow range combination, with one percent and 22 percent improvements, respectively, when compared to the wedge-type vaned diffuser.

INTRODUCTION

The utilization of low solidity diffusers to improve the operating range of centrifugal compressors is well documented. Senoo [1] first introduced the concept in his 1978 patent disclosure where he theorized that the operating range of radial turbomachinery was limited by the physical throat or minimum area location in vaned diffusers and, therefore, could be improved by eliminating the throat. Vaned diffusers are often specified because they offer higher static pressure recovery, hence efficiency, when compared to vaneless diffusers. However, vaned diffusers are also quite sensitive to off-design conditions, thus limiting the useful operating flow range. Useful operating flow range can be defined by the flow ratio at the minimum acceptable efficiency to the flow at surge. Vaneless diffusers, although widely used in many centrifugal compressor applications because of flow range advantages over vaned diffusers, have limited useful operating flow range because the entire level of the efficiency curve is lower (Figure 1).

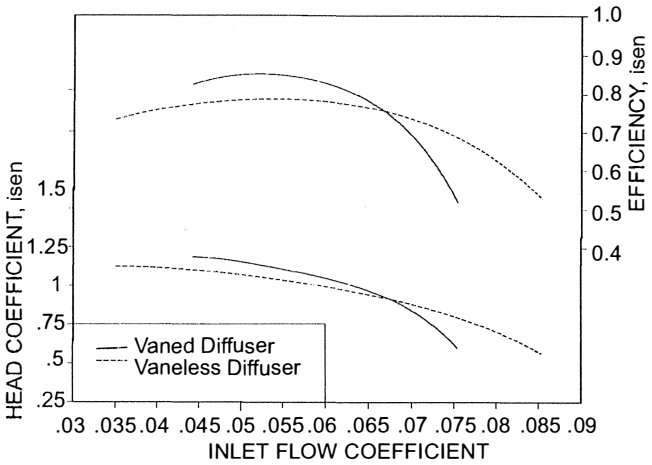

Figure 1. Typical Vaneless vs *Vaned Diffuser Nondimensional Performance.*

Senoo, et al. [2, 3, 4], subsequently applied low solidity diffusers to low specific speed centrifugal blowers and demonstrated that efficiencies approaching that of more traditional vaned diffusers could be achieved, while maintaining nearly the same useful operating flow range vaneless diffusers offered.

Osborne and Sorokes [5] applied low solidity diffusers to the lower specific speed rear stages of an industrial multistage centrifugal compressor using the approximate guidelines established by Senoo. Similar performance improvements were seen during these tests.

Sorokes and Welch [6] used a rotatable low solidity diffuser in a single-stage test rig to understand the important parameters affecting performance. Setting angle or incidence was identified as a critical parameter in this study and optimization yielded improved diffuser performance. However, stage performance remained essentially unchanged despite the improved diffuser performance, most likely indicating a mismatch with the downstream return channel system.

Hohlweg, et al. [7], demonstrated that moderate negative incidence was beneficial when low solidity diffusers were applied

to a high Mach number air compressor. However, incidence had little effect on a low Mach number process compressor that showed significantly less flow range, primarily due to early instability.

Some investigators have used CFD methods to understand the flow physics within these low solidity diffusers and to complement extensive experimental studies. Harada and Goto [8] performed 3-D incompressible viscous flow analysis for both single and tandem low solidity diffusers in a medium specific speed centrifugal compressor. The numerical analysis agreed qualitatively well with experimental data that showed significant performance improvements over a vaneless diffuser.

More recently, Amineni, et al. [9], numerically studied the flow phenomena of low solidity diffusers for an air compressor, experimentally investigated by Hohlweg, using a 3-D compressible viscous CFD code. The authors concluded that the onset of diffuser instability could be qualitatively predicted with this methodology.

Clearly, low solidity diffusers have been applied to a variety of radial turbomachinery and much research and development, both experimental and computational, has been conducted since the 1978 patent disclosure by Senoo. However, it is also clear that many design parameters influence the effectiveness of low solidity diffusers and, therefore, care must be taken when applying the concept, especially for retrofit applications where a number of these critical parameters may be fixed and low solidity diffusers might actually lower performance.

The present study involves the design and retrofit of a low solidity diffuser for a single-stage pipeline centrifugal gas compressor application. Both factory and field testing demonstrated that the compressor, originally designed with a wedge-type vaned diffuser, had impressive efficiency, but with limited useful operating range. The end user desired a wider operating envelope while maintaining the high efficiency. Although a vaneless diffuser could improve the operating range, it most likely would be at the expense of efficiency. Based on the open literature presented previously, a low solidity diffuser certainly has the potential to meet the end user's objective, assuming the existing design envelope does not limit proper selection of the critical design parameters.

The approach taken was to use CFD to analyze the existing impeller in order to establish its discharge boundary condition, which subsequently could be used as the inlet boundary condition for the design and CFD analyses of the candidate diffusers. Although CFD was well established as a viable means to design, analyze, and predict compressor performance [10], factory testing was still considered essential and the final arbiter before recommending hardware changes for a field compressor. Lastly, the selected diffuser configuration was tested in the field to confirm the factory analysis and test results.

PRODUCTION COMPRESSOR

A cross section of the existing production centrifugal compressor is shown in Figure 2. The compressor, designed to boost pressure in a natural gas pipeline, is an axial-inlet, single-stage, overhung rotor configuration. The impeller is backswept 40 degrees from radial, with nine full blades and nine splitter blades, and is shrouded. The inducer hub-to-shroud ratio is 0.61, the inducer shroud to impeller tip radius is 0.59, and the impeller tip width to radius is 0.093. The diffuser is a simple, wedge-type vaned diffuser with 23 vanes as shown in Figure 3. The vaneless space radius and width ratios are 1.15 and 1.05. The diffuser is a parallel wall design with an area ratio of 1.86 and a radius ratio of 1.45. The discharge system is a constant-area collector wrapped forward for compactness.

The nondimensional stage performance shown in Figure 4 is based on both factory and field testing. The stage inlet flow coefficient is 0.055, the isentropic head coefficient is 1.1, and the peak isentropic efficiency is approximately 85 percent. Although the peak efficiency is commensurate with new generation pipeline compressors in the same frame size, the useful flow range is limited by both the efficiency trend with increasing volume flow along with the tested surge line. Assuming a minimum efficiency of 75 percent, the useful operating range to surge is approximately 1.52. In addition, surge margin ranges from 20 to 30 percent within one percent of peak efficiency, which is somewhat narrower than typically desired.

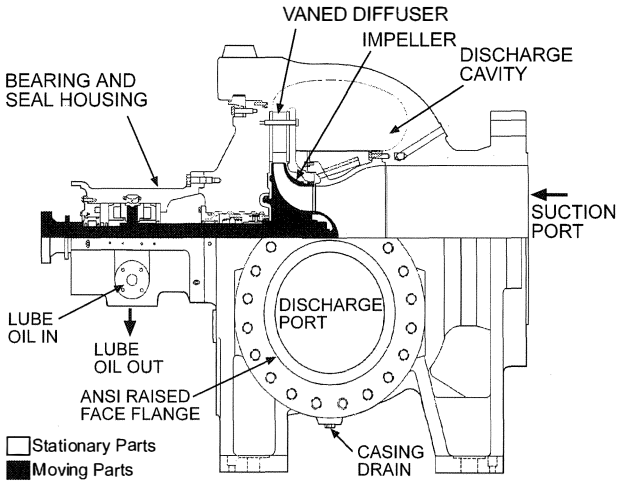

Figure 2. Production Compressor Cross Section.

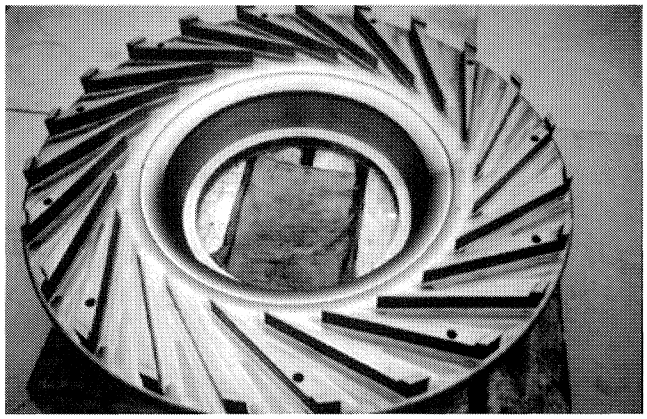

Figure 3. Production Compressor Wedge-Type Vaned Diffuser.

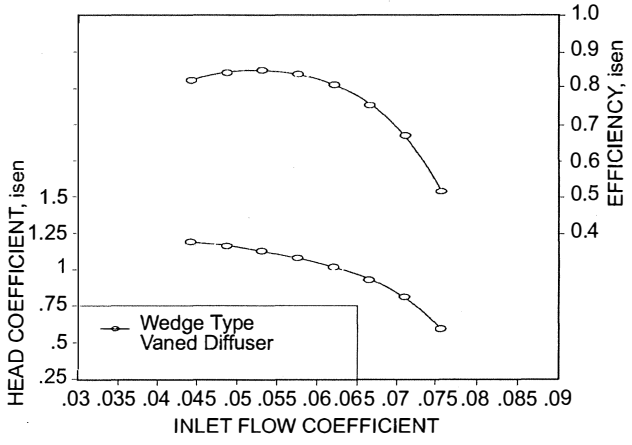

Figure 4. Production Compressor Nondimensional Performance with Wedge-Type Vaned Diffuser.

Impeller Numerical Analysis

The existing impeller was analyzed using BTOB3D [11], a 3-D viscous code that solves the finite volume form of the time dependent Reynolds averaged Navier-Stokes equations with a combined implicit/explicit methodology. The effects of turbulence were modelled using the Baldwin-Lomax [12] algebraic model. BTOB3D, more commonly referred to as the Dawes code, is used primarily in turbomachinery applications. The objective is to compute the impeller discharge velocity profile such that the inlet boundary condition for subsequent diffuser analyses could be conducted. In addition, the impeller itself could be assessed in terms of flowfield structure, because this computational capability did not exist at the time this compressor was designed.

Based on the BTOB3D viscous analysis, the impeller flowfield is relatively well structured. There is evidence of some slight secondary flow from hub to shroud on the suction side as the meridional velocity vectors highlight in Figure 5. The blade-to-blade velocity vectors shown in Figure 6 indicate some secondary flow migration toward the suction side, although this is fairly localized near the shroud. The spanwise or hub-to-shroud discharge flow angle distribution is reasonably constant and, therefore, proper incidence selection is possible using a 2-D diffuser vane.

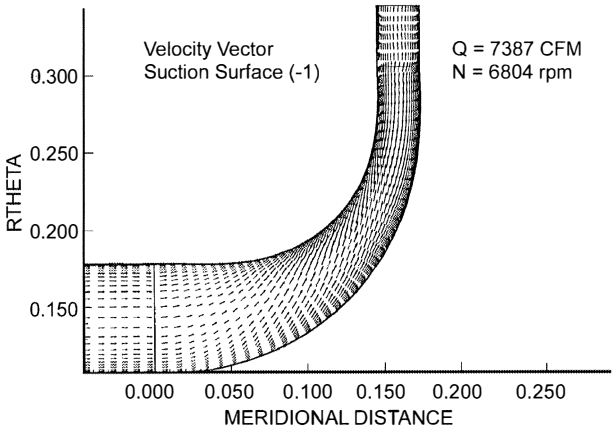

Figure 5. Production Impeller Meridional Velocity Vectors on Suction Side.

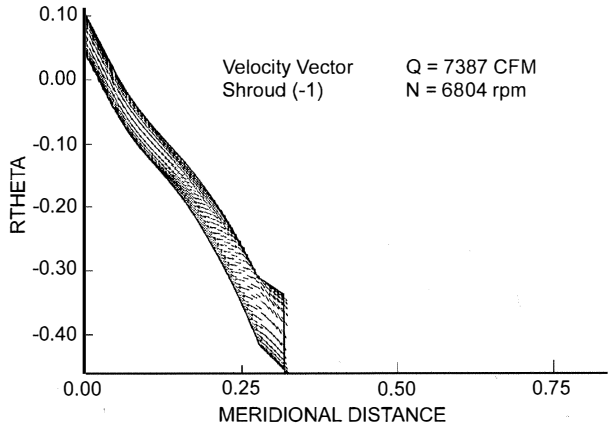

Figure 6. Production Impeller Blade-to-Blade Velocity Vectors at Shroud.

Wedge-Type Vaned Diffuser Analysis

The existing wedge-type vaned diffuser was designed at a setting angle of 68.4 degrees from radial, yielding an incidence of approximately 0.6 degrees when compared to the mass averaged impeller discharge flow angle of approximately 69 degrees derived from BTOB3D. Analysis on the wedge-type vaned diffuser was limited to a quasi 2-D rapid loading calculation [13] in order to focus the majority of effort on developing a replacement diffuser to improve the useful operating flow range.

ALTERNATE DIFFUSER DESIGN AND ANALYSIS

All diffuser configurations were analyzed using a commercially available computational fluid dynamics code [14], which solves the Reynolds stress averaged Navier-Stokes equations in primitive variable form, and is applicable to incompressible and compressible (subsonic, transonic, and supersonic) flows. The effects of turbulence were modelled using the standard k-e turbulence model. Unlike BTOB3D, the commercial CFD code is a general purpose CFD code that allows for modelling of unique and complex geometries.

The computational technique employs an element-based finite volume method. Pressure/velocity coupling is handled using a fourth order pressure redistribution method that is standard for pressure-based (as opposed to density-based, time marching) codes. The domain is subdivided into hexahedral elements, which are the building blocks of the discretization. Volumes are constructed by the appropriate subdivision of the elements. The discretization scheme employed is second order accurate. Its two key components are a directionally sensitive upwind discretization scheme known as linear profile skew (LPS) upwinding, combined with a physically based correction term known as physical advection correction (PAC) [15, 16, and 17]. Together, these schemes reduce solution errors that would naturally arise due to flow directionality and streamwise gradients. The result is a discretization scheme that exhibits very low levels of false total pressure loss, a property that is very important to the present investigation.

In addition to discretization accuracy, the method used to solve the linearized algebraic equations is another factor that is key to the feasibility of the scheme. The commercial CFD code [14] uses an implicit, coupled-iterative solution method that is accelerated by a multigrid method known as additive correction multigrid [18, 19, and 20]. The strengths of this method, from the point of view of the user, are that it is very efficient and robust over a wide range of problems: it requires no user intervention; solution cost increases only linearly with increase in the number of nodes; and it can handle the wide range of control volume sizes and shapes commonly encountered in turbomachinery applications.

Vaneless Diffuser

The vaneless diffuser was created by machining new side plates and outer wall realignment to provide a vaneless space contraction of 10 percent as compared to the expansion of five percent used with the wedge-type vaned diffuser. The vaneless space radius ratio was held constant at 1.15.

The computational domain included the vaneless space contraction, the parallel wall vaneless diffuser, and approximately half of the constant area collector. The corresponding computational grid, shown in Figure 7, used 113 nodes in the streamwise direction, three nodes circumferentially, and 21 nodes spanwise, resulting in a modest problem size of 7,119 nodes. The inflow boundary condition used was the total pressure and direction profile from the BTOB3D impeller analysis. The outflow boundary condition used was mass flow and direction across the outlet face. The remaining boundary conditions include periodicity and smooth walls.

The calculation was run at constant speed for three different mass flows best efficiency point (BEP, $\phi = 0.055$), near stall ($\phi = 0.035$), and near choke ($\phi = 0.085$). The vaneless diffuser meridional velocity vectors are compared in Figures 8, 9, and 10 for the near stall, BEP, and near choke flowrates. The flowfield

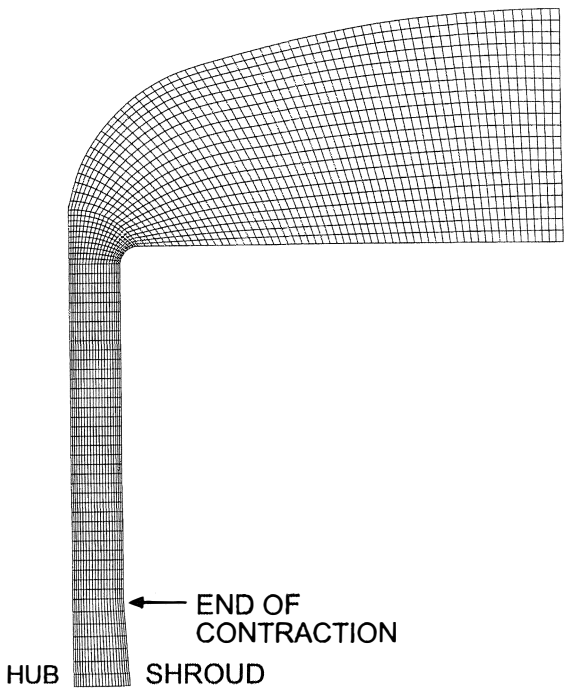

Figure 7. Vaneless Diffuser and Discharge Collector Computational Grid.

becomes more well structured as the flowrate is increased. Even at the BEP, the velocity profile is hub weak, almost to the point of separation as the flow enters the collector. Near stall, reverse flow along the hub wall is evident immediately downstream of the contraction, but recovers before the flow enters the collector.

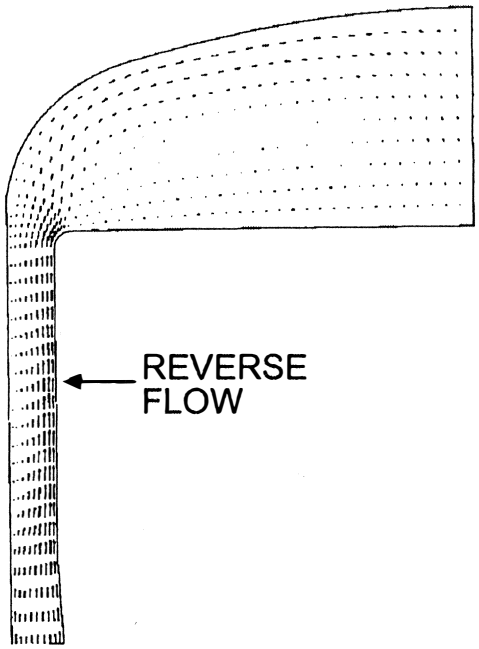

Figure 8. Vaneless Diffuser Meridional Velocity Vectors Near Stall.

One-dimensional parameters were extracted from the 3-D viscous calculation using a weighted mass average. Of particular interest are the vaneless diffuser total pressure loss and static pressure recovery coefficients. These coefficients shown in Figure 11 are rated from the impeller tip to the vaneless diffuser exit, *vs* inlet flow coefficient. Note that the loss is lowest and the pressure

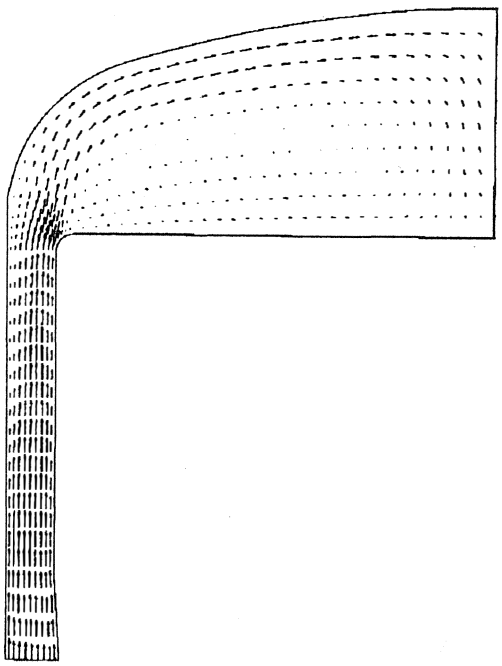

Figure 9. Vaneless Diffuser Meridional Velocity Vectors at Best Efficiency Point.

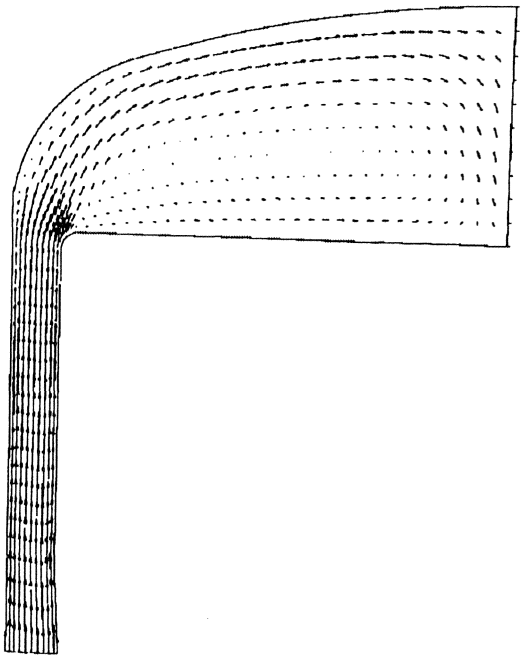

Figure 10. Vaneless Diffuser Meridional Velocity Vectors Near Choke.

recovery is highest at the maximum flow, rather than the desired BEP. Thus, the impeller and vaneless diffuser are somewhat mismatched, resulting in lower efficiency and range potential for the compressor.

The reduced performance expectations of the compressor with the vaneless diffuser are typical in a retrofit situation where the existing mechanical design limits the possible aerodynamic configurations. However, since it was believed that the wedge-type vaned diffuser controlled both surge and choke limits in the original compressor, the vaneless diffuser still offered the potential to improve the useful operating range, albeit at lower peak efficiency levels and was, therefore, further pursued for manufacturing and test.

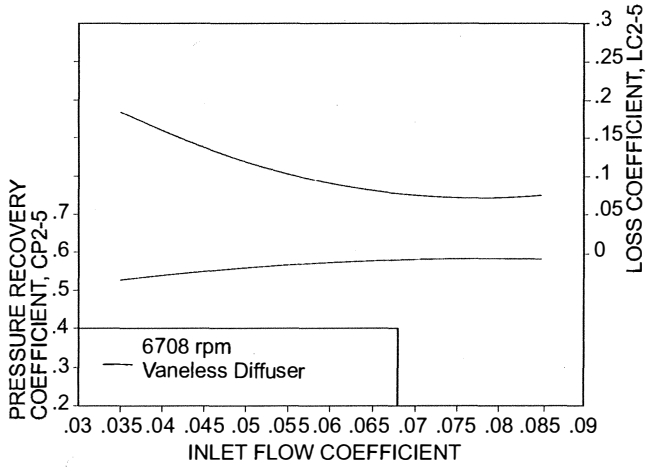

Figure 11. Vaneless Diffuser Static Pressure Recovery and Total Pressure Loss Coefficient.

Flat-Plate Low Solidity Diffuser

The flat-plate low solidity diffuser was created by machining away the majority of the original wedge-type vane, leaving a flat-plate vane in the leading edge region as shown in Figure 12. Note that the local trailing edge regions of six of the original 23 wedge vanes were maintained as standoffs for assembly purposes. Although the flat-plate vane could be made conveniently from the existing wedge vane hardware, most of the key geometric parameters of the wedge-type vane diffuser were essentially fixed, thus limiting the diffuser design options. Of highest concern was the diffuser setting angle that prevents consideration of various incidence levels. In addition, the slight five percent expansion of the vaneless space is somewhat less than desirable. The fixed-vane number more or less sets the vane length or radius ratio when solidity levels on the order of 0.7 are required. The flat-plate vane radius ratio and solidity are 1.093 and 0.77, as compared to the wedge type vane at 1.45 and 2.64. Clearly, the flat-plate configuration would be different in some aspects if this were a new design rather than a retrofit; however, the specified geometry was well within the boundaries of some successful low solidity diffusers presented in the open literature.

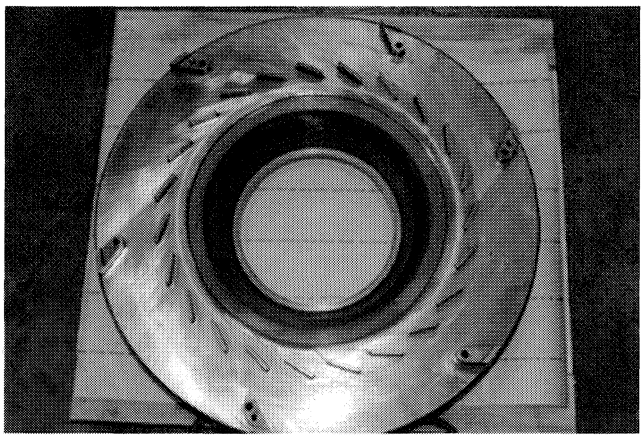

Figure 12. Flat-Plate Low Solidity Diffuser.

The computational domain included the vaneless space expansion, the parallel wall flat-plate low solidity diffuser, the downstream parallel wall vaneless diffuser, and approximately half of the constant area collector. The corresponding computational grid uses 127 nodes in the streamwise direction, 27 nodes circumferentially, and 25 nodes spanwise, resulting in a problem size of 85,725 nodes. The boundary conditions used were identical to the vaneless diffuser calculation with the addition of blockoffs for the pressure and suction sides of the vane.

The calculation was run at constant speed for three different mass flows: best efficiency point ($\phi = 0.055$), near stall ($\phi = 0.040$), and near choke ($\phi = 0.085$). Note that the near stall condition was at a slightly higher flowrate than the vaneless diffuser calculation. Vane-to-vane midspan velocity vectors at the near stall, BEP, and near choke flowrates are shown in Figures 13, 14, and 15. The flowfield is generally well structured with some slight negative incidence effects noted for the near choke condition. Since the near stall and BEP flow coefficients are only slightly different, the flowfield results are expectedly similar.

The extracted 1-D total pressure loss and static pressure recovery coefficients are shown in Figure 16 *vs* inlet flow coefficient. The diffuser performance is rated from the impeller tip to the downstream vaneless diffuser exit in order to compare with the fully vaneless diffuser calculations. The flat-plate, low solidity diffuser has minimum total pressure loss and maximum pressure recovery at BEP, indicating a proper impeller/diffuser match. As expected, the total pressure losses are higher than the equivalent vaneless diffuser, but not so expectedly, the static pressure recovery is only higher around BEP. At off-design flowrates, especially at higher flows, the flat-plate low solidity diffuser has lower static pressure recovery, possibly indicating incidence effects play a large role in low-solidity diffuser performance.

The sensitivity to incidence is a function of the inherently diffusing flow and a relatively blunt vane leading edge. Unfortunately, the derived flat-plate design with fixed vane number essentially sets the minimum thickness required for structural integrity in the field. Looking at only the flat-plate low solidity diffuser performance, one might conclude that only marginal improvement over the vaneless diffuser can be expected. However, the downstream collector performance may improve with a lower entering velocity and a more favorable entry flow angle. The expected improvement in collector performance, coupled with the significantly improved peak efficiency based on the CFD analysis, resulted in further pursuing the flat-plate low solidity diffuser configuration for manufacturing and test.

Airfoil-Type Low Solidity Diffuser

Unlike the flat-plate configuration, the airfoil-type low solidity diffuser could be designed with reasonable geometric freedom, including setting angle, vane shape, vane number, vane thickness, radius ratio, and solidity. In addition, the airfoil-type design could benefit from the completed flat-plate configuration CFD analyses, which highlighted concerns about off-design performance.

The first fundamental decision made was to use an airfoil-shaped vane to better accommodate the off-design incidence with thickness variation. Assuming the vaneless space dimensions are maintained as in the vaneless diffuser, the next decision was solidity level, which is primarily a function of vane chord (radius ratio) and number. The open literature tends to favor fewer and longer vanes for a given solidity level, which also benefits field durability and aerodynamic performance. The solidity of the flat-plate design was approximately maintained but the vane number was reduced to 11, which corresponds to an airfoil vane chord roughly twice that of the flat-plate vane.

The vane thickness profile was then selected to provide a maximum thickness to chord ratio of approximately 11 percent, located near midchord to allow a through hole for bolting to the diffuser back plate along with structural integrity. In order to experimentally evaluate the sensitivity to incidence, the vanes were milled separately such that various installation arrangements could be assembled for alternate setting angle tests. The vanes could be pinned on either side as shown in Figure 17, which allowed examination of the nominal setting angle of 71 degrees (minus two degrees incidence) along with plus/minus four degrees

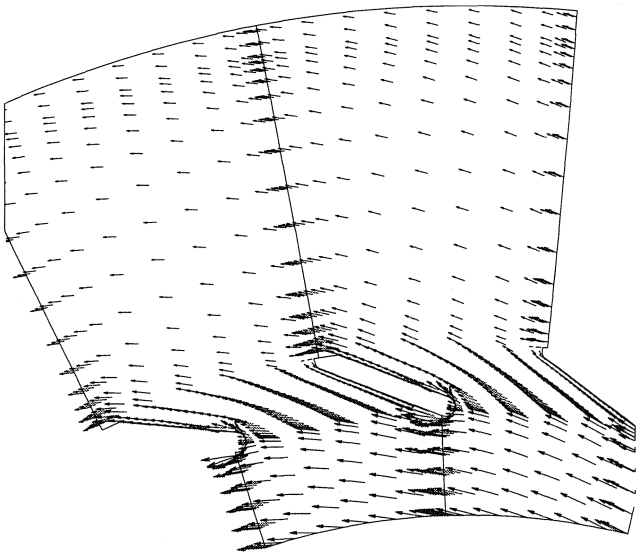

Figure 13. Flat-Plate Low Solidity Diffuser Vane-to-Vane Velocity Vectors Near Stall.

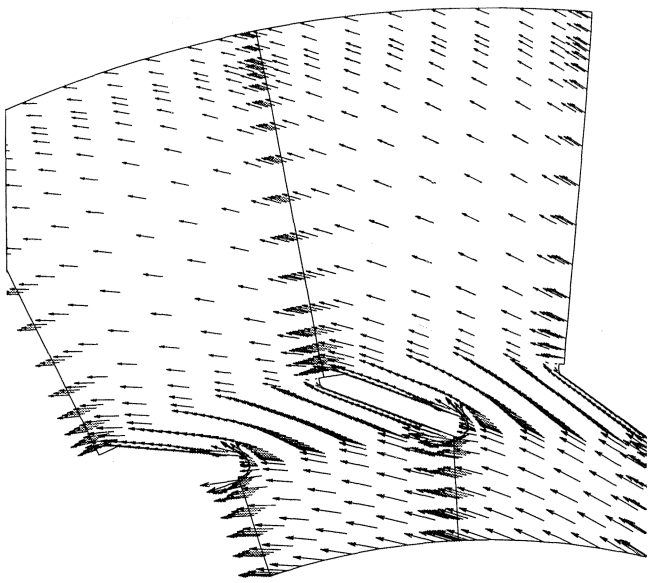

Figure 14. Flat-Plate Low Solidity Diffuser Vane-to-Vane Velocity Vectors at Best Efficiency Point.

incidence variation from nominal. As was the case with the flat-plate configuration, the local trailing edge regions for six of the original 23 wedge vanes were maintained as standoffs for assembly purposes.

The computational domain included the vaneless space contraction, the parallel wall airfoil-type low solidity diffuser (nominal setting angle), the downstream parallel wall vaneless diffuser, and approximately half of the constant area collector. The corresponding computational grid uses 127 nodes in the streamwise direction, 27 nodes circumferentially, and 25 nodes spanwise, resulting in a problem size of 85,725 nodes. The boundary conditions used were identical to the flat-plate low solidity diffuser calculation.

The calculation was run at constant speed for six different mass flows ranging from near stall ($\phi = 0.035$) to near choke ($\phi = 0.085$), including the best efficiency point ($\phi = 0.055$). The vane-to-vane midspan velocity vectors are shown in Figures 18, 19, and 20 for the near stall, BEP, and near choke flowrates. Consistent with the flat-plate low solidity at near stall and BEP, the flowfield is well

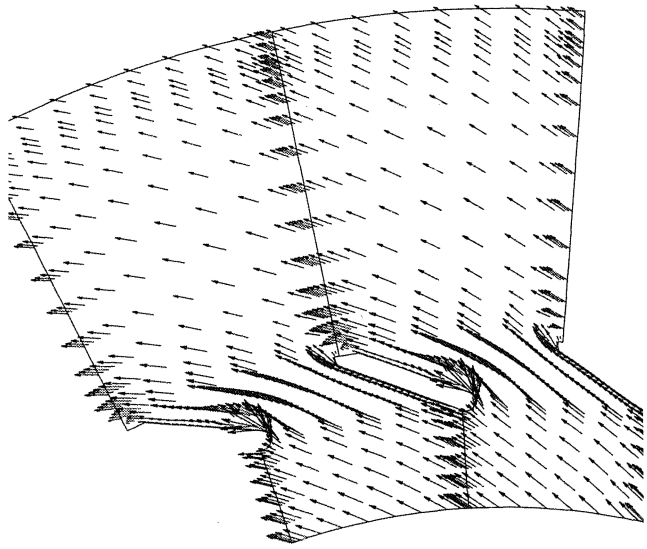

Figure 15. Flat-Plate Low Solidity Diffuser Vane-to-Vane Velocity Vectors Near Choke.

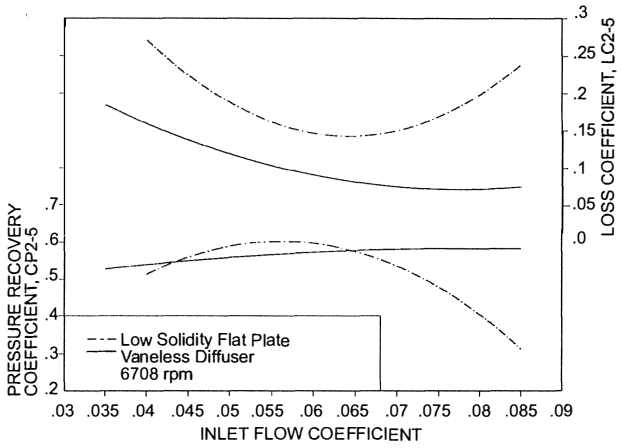

Figure 16. Flat-Plate Low Solidity Diffuser Static Pressure Recovery and Total Pressure Loss Coefficient Compared with Vaneless Diffuser.

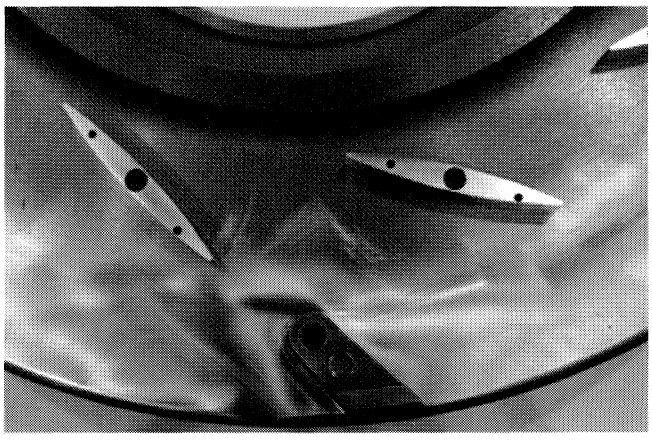

Figure 17. Airfoil-Type Low Solidity Diffuser.

structured for the incidence swing of plus six to minus two degrees. However, there is some evidence of local recirculation at the suction side trailing edge. Near choke, where the incidence is about −20 degrees, there is reverse flow along the entire pressure side of the vane.

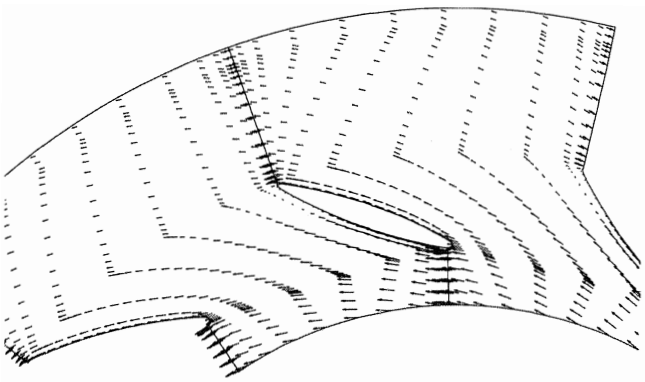

Figure 18. Airfoil-Type Low Solidity Diffuser Vane-to-Vane Velocity Vectors Near Stall.

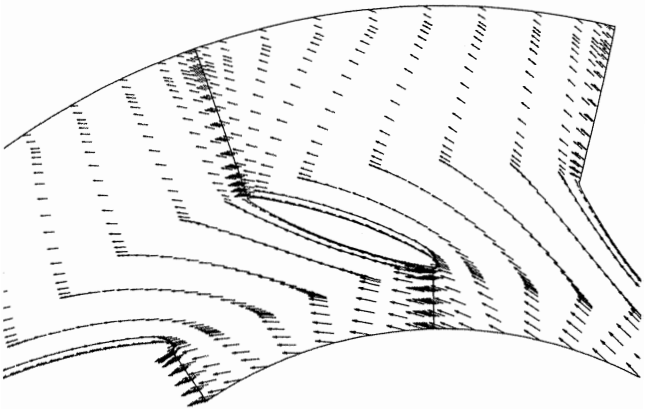

Figure 19. Airfoil-Type Low Solidity Diffuser Vane-to-Vane Velocity Vectors at Best Efficiency Point.

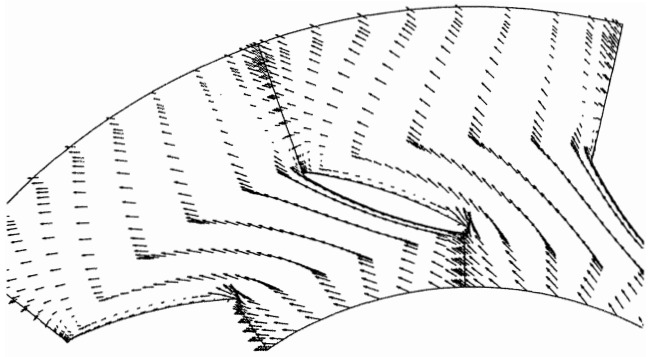

Figure 20. Airfoil-Type Low Solidity Diffuser Vane-to-Vane Velocity Vectors Near Choke.

The extracted 1-D total pressure loss and static pressure recovery coefficients *vs* inlet flow coefficient are shown in Figure 21. The impeller and airfoil-type low solidity diffuser are well matched because the total pressure loss is minimum and the static pressure recovery is maximum at BEP. When compared to the flat-plate low solidity diffuser, the airfoil type has lower total pressure loss over most of the flow range and higher static pressure recovery over the entire flow range. When compared to the vaneless diffuser, the airfoil type has higher total pressure loss for all flowrates, but with lower static pressure recovery only near choke. As with the flat-plate configuration, this result is generally expected because of incidence effects, and since the vaneless diffuser performance improves as flowrate is increased. However, the static pressure recovery improves rapidly as the flowrate is reduced, indicating that the airfoil-type low solidity diffuser has the highest efficiency and range potential based on the CFD analyses.

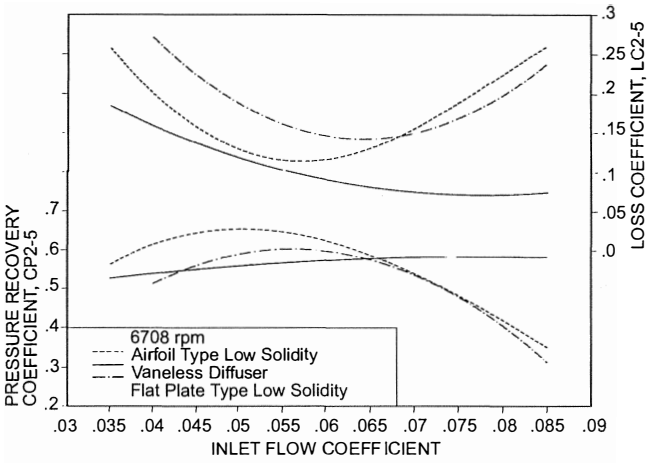

Figure 21. Airfoil-Type Low Solidity Diffuser Static Pressure Recovery and Total Pressure Loss Coefficient Compared with Vaneless Diffuser and Flat-Plate Low Solidity Diffuser.

EXPERIMENTAL INVESTIGATION

The test facility used in this study is an open-loop arrangement capable of testing in accordance with ASME PTC-10 [21]. All of the diffuser configurations were tested in the same full-size "production" compressor (Figure 22) in order to more closely represent the "as-installed" field compressor. The test compressor is driven by a slave gas turbine engine capable of delivering greater than 1000 hp at 22,300 rpm. A reduction gearbox is also used to match the gas turbine to the compressor maximum continuous speed of 9500 rpm. Both the driver and compressor skids were fully instrumented for operation and control along with compressor mechanical and aerodynamic performance.

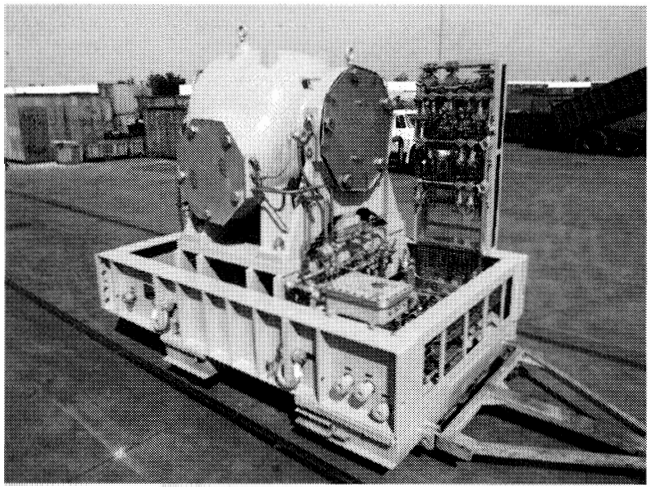

Figure 22. Typical Full-Size Slave Compressor for Diffuser Testing.

Ambient air is ingested through a flow measuring venturi and inlet duct. The compressed air is exhausted through a discharge duct and back-pressuring throttle valve before being muffled back to atmosphere. The inlet and discharge ducts were sized to be three times their respective diameters and were used as instrumentation spools for temperature and pressure measurement. Standard compressor instrumentation includes temperature, pressure, flow, speed, and vibration.

Instrumentation

Temperature measurements included four resistance temperature detectors (RTDs) at both compressor suction and discharge: one RTD at the venturi throat; Type K thermocouples for the radial bearing lube oil inlet and drain; and one Type K thermocouple for the seal gas vent. Pressure measurements include four Kiel probes at both compressor suction and discharge; and two delta pressure velocity at the venturi throat. Flow measurements include compressor flow from the venturi; radial and thrust bearing lube oil flow with turbine flowmeters; and seal gas vent flow with rotometers. Vibration measurements include both X and Y probes for the radial bearing. Speed is measured using a key phasor.

Test Procedure

The compressor and discharge piping were covered with thermal blankets to minimize heat transfer effects. The compressor was operated for one hour prior to aerodynamic testing for heat soaking purposes. Testing was conducted at three rotational speeds (5,324, 6,708, and 8,092 rpm), each from choke to surge with a minimum of eight operating points per speed line. These speeds represent the equivalent air speeds when compressing air rather than natural gas. Steady-state conditions were typically reached 30 minutes after reaching the desired operating point. Multiple data points at each flow/speed condition and repeat tests were conducted to ensure a data accuracy of approximately plus/minus two percent.

Test Results

Test results are presented only for the equivalent air design speed of 6,708 rpm, because within the machine Mach number limits tested, single-stage pipeline compressors of this kind obey the fan law; therefore, nondimensional results are essentially the same. The tested nondimensional performance results of all diffuser configurations are shown in Figure 23. The production compressor with the wedge-type vaned diffuser demonstrated a high peak efficiency albeit with modest surge margin. The useful flow range from 75 percent efficiency to surge was approximately 1.52.

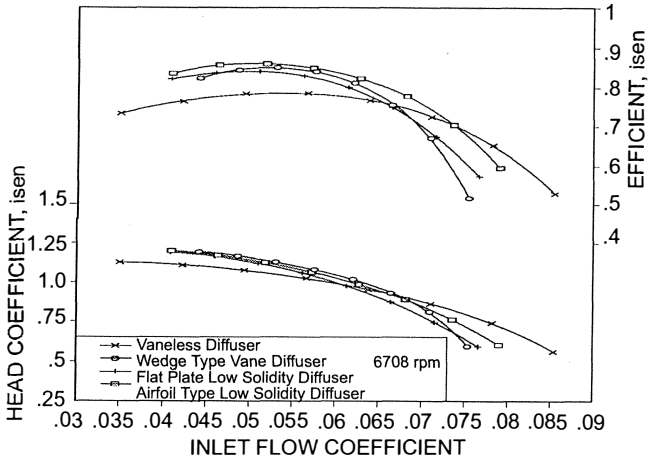

Figure 23. Nondimensional Test Results for All Diffuser Configurations.

As expected from the CFD analysis, the compressor efficiency with the vaneless diffuser configuration was significantly lower, approximately eight percent than the production compressor. However, the vaneless configuration did improve the useful flow range by nearly 26 percent. It was also evident from this test that the original wedge-type vaned diffuser controlled the surge limit in the production compressor because the surge flow improved substantially with the vaneless configuration. The flow at 75 percent efficiency was nearly the same as the production compressor, indicating the improved useful flow range was derived solely from the lower surge flow.

The peak compressor efficiency with the flat-plate low solidity diffuser proved to be within approximately one percent of the production compressor. The useful flow range improved by approximately 12 percent, primarily due to a more favorable surge flow as was the case with the vaneless diffuser. However, the location of peak efficiency shifted consistently with the surge flow improvement. The flow at 75 percent efficiency was slightly less than the vaneless configuration and, interestingly, the wedge-type vaned configuration as well. Only a marginal increase in maximum flow capacity was noted relative to the production compressor.

The airfoil-type low solidity diffuser at the nominal setting angle yielded the best overall compressor performance as was anticipated from the CFD analyses. Relative to the production compressor, the peak efficiency improved by approximately one percent and the useful flow range improved by approximately 22 percent. Unlike the flat-plate low solidity configuration, the improvement in flow range was derived both from reduced surge flow and increased flow capacity. The surge flow was nearly the same as the flat-plate results, but the flow at 75 percent efficiency was significantly higher than all previous diffuser arrangements.

Test results for the modified setting angles are shown in Figure 24 *vs* the nominal setting angle of 71 degrees (minus two degrees incidence). The flatter or more tangential setting angle of 75 degrees reduced peak efficiency by about four percent. Both the surge flow and the flow at 75 percent efficiency were reduced by approximately 10 percent, resulting in nearly the same useful flow range. The more radial-setting angle of 67 degrees improved the useful range by five percent, due to increased flow at 75 percent efficiency without a similar shift in surge flow. The peak efficiency level remained essentially the same.

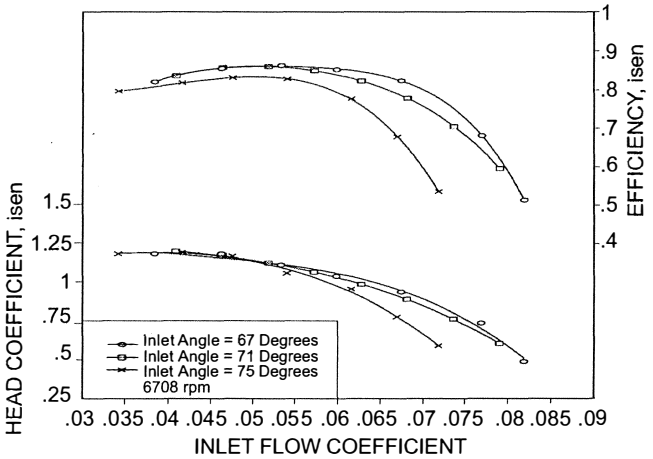

Figure 24. Nondimensional Test Results for Alternate Setting Angles of Airfoil-Type Low Solidity Diffuser.

FIELD RETROFIT

The airfoil-type low solidity diffuser configuration yielded superior compressor performance. Furthermore, test results with the 67 degree setting angle (plus two degrees incidence) provided the best combination of efficiency and useful flow range for the airfoil-type low solidity diffuser. Clearly, with all things being equal, the airfoil type would be the diffuser configuration of choice for the field retrofit. However, the end user desired a fast turnaround and only had a very limited window to perform the hardware exchange that required the availability of a field-ready diffuser. The airfoil-type vanes were manufactured individually to facilitate assembly at various setting angles and were not suitable for immediate field installation.

The flat-plate low solidity diffuser, although not as attractive as the airfoil type from a performance perspective, was made from the production wedge-type vaned diffuser and still offered significant performance benefits over the production wedge-type vaned diffuser. In order to ensure field readiness, both modal analysis and testing of the flat-plate vanes were conducted simultaneously with the aerodynamic development effort and showed relatively low inherent damping (higher amplification factors) and, therefore, higher than desired potential dynamic stresses at resonance. A slot was milled in the top of each vane (Figure 25) to house Teflon® friction dampers to lower the amplification factor and, thus, dynamic stresses. Modal testing confirmed significantly improved damping characteristics and increased the factor of safety to 15.

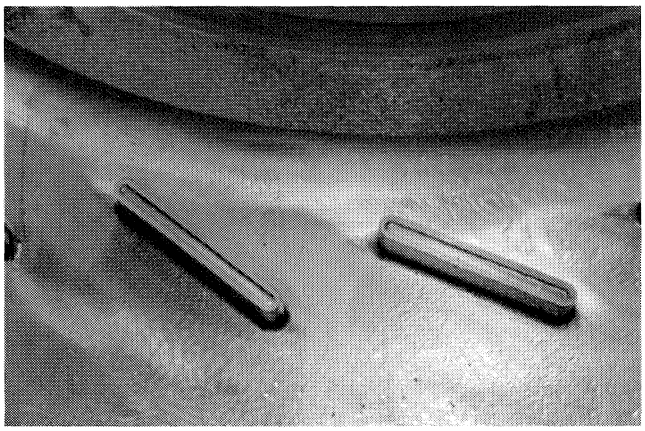

Figure 25. Milled Slot for Teflon® Insert on Flat-Plate Low Solidity Diffuser Vane.

The end user and original equipment manufacturer (OEM) agreed on the flat-plate low solidity diffuser configuration and to an installation procedure that accounted for the critical nature of the downtime. A field performance test agenda was prepared by the OEM prior to field installation that included an expected field performance map based on the factory test results. The end user set both flow and head tolerance levels to be plus or minus four percent, which essentially bracketed the efficiency and surge location. The field test agenda was derived to replicate and confirm the factory test results. Both the field test agenda and the associated performance map were agreed upon prior to installation.

In order to minimize downtime, all tools, parts, and personnel were onsite prior to station shutdown. The flat-plate, low solidity diffuser with the Teflon® friction dampers was installed in the field compressor. The removal of the drive shaft and aerodynamic bundle was completed on the driven skid. The mechanical arrangement of the compressor was fairly straightforward and, accordingly, the complete diffuser retrofit took approximately 24 hours to complete.

Although a field performance test was planned that replicated the factory test, the end user had operational requirements that precluded a full evaluation. However, in order to demonstrate the factory-tested surge line improvement, the compressor was throttled at 7157 rpm until the flow had reached the original surge line of the production compressor. The flow was further reduced in small increments until steady operation of the compressor was achieved at 12 percent lower flow, confirming the factory test results. The efficiency level was measured at selected operating points as the compressor was throttled to surge. Tested peak efficiency was about one percent higher than the factory test results. The end user accepted the performance results that showed improvements in both the surge line and efficiency level. The pipeline gas compressor with the retrofitted low solidity vane diffuser has been in service for more than three years with no reported issues.

CONCLUSIONS

Discussed herein were the design and retrofit of low solidity diffusion concepts to a pipeline centrifugal gas compressor field application. The major conclusions are as follows:

- The open literature presented many studies that demonstrated the successful application of low solidity diffusion to radial turbomachinery. However, it was also clear that without proper design and analysis techniques, low solidity diffusers may actually reduce performance.
- CFD can be used quite effectively in the design and analysis of centrifugal compressor components. This was particularly important in the development of the airfoil-type low solidity diffuser where more design degrees of freedom were available to improve performance.
- Design choices can be significantly limited in retrofit situations. This was the case with both the vaneless and flat-plate low solidity diffuser configurations and, to a lesser degree, with the airfoil-type low solidity diffuser. Thorough analysis was required to determine if reasonable performance improvements could be realized in light of these limitations.
- A very effective, airfoil-type low solidity diffuser was developed that demonstrated both improved efficiency and useful flow range relative to the production compressor. However, the flat-plate low solidity diffuser was used for the field retrofit because it met the end user's requirements for both rapid production readiness and sufficient performance improvement.

NOMENCLATURE

ϕ = Flow coefficient, $Q/[(\pi(D_2^2/4)]U_2$

Q = Volume flow (cfm)

D = Diameter (inches)

P = Pressure (psia)

U = Impeller wheel speed (fps)

ψ = Head coefficient, $H_{is}/(U_2^2/2g)$

H = Head (ft-lbf/lbm)

g = Gravitational constant

η = Efficiency, $Pr^{k-1/k}-1/(Tr-1)$

Pr = Pressure ratio, P_e/P_i

k = Specific heat ratio

Tr = Temperature ratio, T_e/T_i

LC = Total pressure loss coefficient $(Pt_{in}-Pt_{out})/(Pt_{in}-Ps_{in})$

C_P = Static pressure recovery $(Ps_{out}-Ps_{in})/(Pt_{in}-Ps_{in})$

Subscripts:

1 = Impeller inlet

2 = Impeller exit

5 = Diffuser exit

in = Component inlet

out = Component exit

i = Compressor inlet

e = Compressor exit

is = Isentropic

REFERENCES

1. Senoo, Y., Japanese Patent Application Disclosure 119411/78, in Japanese (October 1978).

2. Senoo, Y., "Low Solidity Circular Cascade for Wide Flow Range Blower," Proceedings of Advanced Concepts in Turbomachinery, Fluid Dynamics Institute, Hanover, New Hampshire (August 1981).

3. Senoo, Y., Hayami, H., and Ueki, H., "Low Solidity Tandem Cascade Diffusers for Wide Flow Range Centrifugal Blowers," ASME Paper Number 83-GT-3 (1983).

4. Senoo, Y., "Low Solidity Cascade Diffusers for Wide Flow Range Centrifugal Blowers," Flow in Centrifugal Compressors, VKI Lecture Series 1984-07 (May 1984).

5. Osborne, C. and Sorokes, J. M., "The Application of Low Solidity Diffusers in Centrifugal Compressors," ASME FED, *69* (1988).

6. Sorokes, J. M. and Welch, J. P., "Experimental Results on a Rotatable Low Solidity Vaned Diffuser," ASME Paper Number 92-GT-19 (1992).

7. Hohlweg, W. C., Direnzi, G. L., and Aungier, R. H., "Comparison of Conventional and Low Solidity Vaned Diffusers," ASME Paper Number 93-GT-98 (1993).

8. Harada, H. and Goto, M., "Numerical and Experimental Studies of Single and Tandem Low Solidity Cascade Diffusers in a Centrifugal Compressor," ASME Paper Number 93-GT-108 (1993).

9. Amineni, N. K., Engeda, A., Hohlweg, W. C., and Boal, C. F., "Flow Phenomena in Low Solidity Diffusers of an Air Packaging Compressor," ASME Paper Number 95-WA/PID-1 (1995).

10. Flathers, M. B. and Baché, G. E., "Aerodynamically Induced Radial Forces in Centrifugal Gas Compressor—Part 2: Computational Investigation," ASME Paper Number 96-GT-352 (1996).

11. Dawes, W. N., "Development of a 3D Navier-Stokes Solver for Application to All Types of Turbomachinery," ASME Paper Number 88-GT-70 (1988).

12. Baldwin, B. and Lomax, H., "Thin Layer Approximation and Algebraic Model for Separated Turbulent Flows," AIAA Paper Number 78-257 (1978).

13. Howard, J. H. G., Osborne, C., and Japikse, D., "A Rapid Loading Procedure for Centrifugal Impeller Design," ASME Paper Number 94-GT-148 (1994).

14. TASCflow Users Manual, Version 2.2, Advanced Scientific Computing (1993).

15. Galpin, P. F., Huget, R. G., and Raithby, G. D., "Fluid Flow Simulations in Complex Geometries," Paper presented at the CNS/ANS Conference on Simulation Methods in Nuclear Engineering, Montreal (1986).

16. Schneider, G. E. and Raw, M. J., "A Skewed, Positive Influence Coefficient Upwind Procedure for Control Volume-Based Element Convection-Diffusion Computations," Numerical Heat Transfer, *8*, pp. 1-26 (1986).

17. Van Doormaal, J. P., Turan, A., and Raithby, G. D., "Evaluation of New Techniques for the Calculation of Internal Recirculating Flows," AIAA Paper Number 87-0059, 25th Aerospace Sciences Meeting, Reno, Nevada (1987).

18. Van Doormaal, J. P., Hutchinson, B. R., and Turan, A., "An Evaluation of Techniques Used to Accelerate Segregated Methods for Predicting Viscous Fluid Flow," AIAA Paper Number 86-1653, presented at the AIAA/ASME/SAE/ASEE 2nd Joint Propulsion Conference, Huntsville, Alabama (1986).

19. Hutchinson B. R., and Raithby, G. D., "A Multigrid Method Based on the Additive Correction Strategy," Numerical Heat Transfer, *9*, pp. 511-537 (1986).

20. Hutchinson, B. R., Galpin P. F., and Raithby, G. D., "Application of Additive Correction Multigrid to the Coupled Fluid Flow Equations," Numerical Heat Transfer, *13*, pp. 133-147 (1988).

21. American Society of Mechanical Engineers, "Compressors and Exhausters—Power Test Code," PTC-10, 1965 Edition, Reaffirmed 1974 and 1986.

ACKNOWLEDGEMENTS

The author would like to acknowledge the efforts of Frank Shih and Jeff Moore who assisted with the analysis and the factory testing, George Baché who provided guidance with the computational studies, and Tim David and Ed Fowler who assisted with the generation of the figures. The author would also like to thank Solar Turbines Incorporated for the permission to publish this paper.